

Electrochemical texturing of Al-doped ZnO thin films for photovoltaic applications

Sebastian O. Klemm · Sascha E. Pust ·
Achim Walter Hassel · Jürgen Hüpkas ·
Karl J. J. Mayrhofer

Received: 19 November 2010 / Revised: 12 January 2011 / Accepted: 13 January 2011 / Published online: 12 February 2011
© Springer-Verlag 2011

Abstract The processes during chemical and electrochemical etching of Al-doped ZnO are investigated utilizing a scanning flow cell setup with online detection of dissolved Zn ions. The rate of chemical dissolution was found to be a linear function of buffer and proton concentration in near neutral pH solutions according to a transport limited reaction. In contrast, electrochemical etching is limited by the kinetics of the reaction and increases linearly with the imposed current density. Due to this fundamental difference, the dissolution of Zn can be either uniform over the whole surface or highly localized at active sites like grain boundaries. A combined approach of chemical etching and the well-controllable galvanostatic dissolution thus allows a fine adjustment of the ZnO:Al surface texture for applications in silicon thin film photovoltaic cells in order to improve their overall energy conversion efficiency.

Keywords Photovoltaics · ZnO thin film · ZnO dissolution · Electrochemical texturing · Microelectrochemistry

Introduction

Photovoltaic energy conversion is a key approach towards sustainability of humanity and conservation of valuable natural resources [1]. The improvement of both crystalline silicon and thin film solar cells has therefore attracted great interest over the last decade. Especially thin film solar cells offer a large potential regarding cost reduction and mass fabrication [2, 3], however still lack in energy conversion efficiencies compared to other more expensive technologies. The introduction of thin layers of rough ZnO as a front contact and as a part of the back reflector in Si thin film solar cells can significantly reduce this drawback [4]. While ZnO meets the high demands regarding optical transparency, electrical conductivity, and material properties regarding the growth of the Si absorber layers, it additionally provides light scattering that can lead to a considerable improvement of the overall solar energy utilization given an appropriate texture [5–7]. Figure 1 schematically describes a setup of a Si thin film solar cell with Al-doped ZnO front and back contacts (ZnO:Al), which has been deposited starting from the side of the incident light in the so-called superstrate configuration.

Incident light scatters at the interface of the front ZnO:Al contact with the actual absorber material, thus prolonging its path through the intrinsic Si layer and hereby increasing the probability of absorption. The light scattering effect is depended on the interface morphology and is generally achieved by an artificial roughening of the deposited ZnO surface utilizing a chemical etching step in diluted hydrochloric acid [6]. This results in crater-like structures in the ZnO:Al film with typical diameters of approximately 1 μm at surface roughnesses of $\text{RMS} \approx 135 \text{ nm}$ depending on the deposition and etching parameters. The additional texture is

S. O. Klemm (✉) · A. W. Hassel · K. J. J. Mayrhofer
Max-Planck Institut für Eisenforschung,
Max-Planck Str. 1,
40237 Düsseldorf, Germany
e-mail: klemm@mpie.de

S. E. Pust · J. Hüpkas
Forschungszentrum Jülich GmbH, IEK5–Photovoltaik,
52425 Jülich, Germany

A. W. Hassel
Institute for Chemical Technology of Inorganic Materials,
Johannes Kepler University,
Altenberger Str. 69,
4040 Linz, Austria

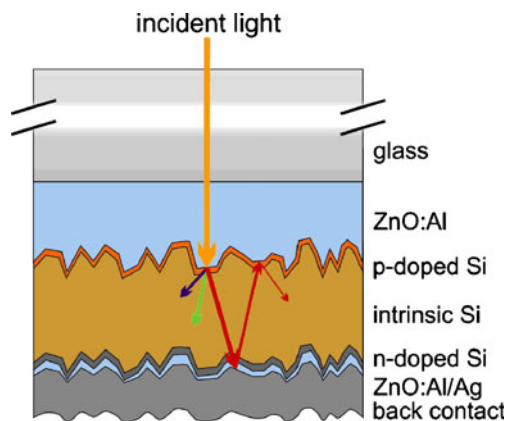


Fig. 1 Schematic drawing of a Si thin film solar cell in superstrate configuration with indication of the light scattering effect at the rough ZnO–Si interface

visible to the naked eye as a slight milkiness (haze) and increases the short circuit current of microcrystalline Si thin film solar cells up to about 45% compared to solar cells on as-deposited ZnO:Al [7]. The etch process is constantly optimized with respect to the optical and electrical performance of the ZnO:Al film, as it is significantly influenced by the material properties of the film [8, 9] as well as by the choice of the etching agent [10]. However, a detailed understanding of the relationship between etching conditions, surface/interface structure, and photovoltaic performance is still lacking, thus inhibiting a more systematic approach for the texturing of ZnO films.

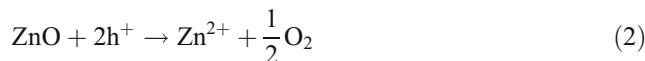
The etching mechanism on single crystalline ZnO is well understood since the early 1960s [11, 12] and can be explained based on a dangling bond model initially proposed for III-V semiconductors [13]. The kinetics of the so-called chemical etching, i.e., the chemically induced conversion of ZnO into soluble complexes, has been investigated early by Fruhwirth [14] and Gerischer [15] and proceeds according to Eq. (1) in acidic media.



An analogous reaction with hydroxyl ions as etching agent forming $[\text{Zn}(\text{OH})_{2+x}]^{-x}$ ($X=1$ or 2) species is possible due to the amphoteric character of zinc and can be utilized as an etching process as well [16, 17]. Even though this amphoterity causes the conditions for thermodynamic stability of ZnO to be fairly narrow (e.g., around pH 8–11 without contribution of other ions [18, 19]), low dissolution rates are observed under moderate conditions due to either slow kinetics [20] or transport limitations [21].

A dissolution process of so far minor relevance is the etching of ZnO by the anodization technique, which

can lead to both oxide lattice decomposition and water oxidation according to Eqs. (2) and (3), respectively [22].



The reaction is driven by hole generation through tunneling processes and has been found to be promoted by increasing dopant concentrations [23]. For polycrystalline substrates like the sputter deposited ZnO:Al in this paper with a high degree of intrinsic heterogeneity and a significant number of defects [24], however, the etch processes are far more complex. Since no defined Zn- or O-termination is achieved due to the different grain orientation in sputter deposited samples, the etching mechanism cannot be discussed in terms of the crystalline orientation despite the fact that the etching of ZnO is highly sensitive to its microstructure [25, 26].

In the present work, the electrochemical and chemical characterization of ZnO:Al dissolution is combined with online measurement of the Zn dissolution rate and scanning electron microscopy post-analysis, in order to improve the understanding of the involved processes and the influence of the various texturing parameters. While this approach could be applied to any kind of sample, particular focus is put on RF-sputtered ZnO:Al thin films that are known to exhibit structured surfaces with grains in the 10–100 nm range and a c -axis directed along the surface normal [27, 28]. A fully automated, microelectrochemical scanning flow cell setup [29] is used to precisely address particular locations with a diameter of around 200 μm on a thin film sample and coupled with an UV–VIS spectrometer for online monitoring of zinc concentration in the electrolyte.

Experimental section

Fabrication of Al-doped ZnO thin films and profilometry Polycrystalline and approximately 800 nm thick ZnO:Al films were deposited on a cleaned (10×10) cm^2 glass substrate (Corning Eagle XG) using radio frequency magnetron sputtering in a vertical in-line system (VISS 300, VON ARDENNE Anlagentechnik GmbH, Dresden, Germany) from a ceramic target consisting of ZnO with 1 w/w% Al_2O_3 (Cerac inc. Milwaukee, WI, USA). The deposition was carried out at a substrate temperature of 300 $^\circ\text{C}$, a discharge power of 2 W cm^{-2} , and an Ar pressure

of 0.1 Pa. Details about the process were published elsewhere [30].

Surface profilometric measurements were performed with a Dektak 6m Stylus Profiler (Veeco, Santa Barbara, CA, USA), using a stylus with a radius of 12.5 μm and a lateral step size of 0.33 μm . The data has been leveled by subtracting a linear background. Additionally, the curves were smoothed with a weighted moving average over a range of 15 data points for noise reduction.

Electrolyte preparation and electrochemical setup The electrolytes were prepared from ultrapure deionized water (PureLab Plus, Elga, Celle, Germany) and p.a. grade chemicals (Merck KGaA, Darmstadt, Germany). Acetate buffers were prepared by dissolving 0.1 M sodium acetate and adjusting the pH by addition of 0.1 M HCl as monitored by a glass electrode (E-632 Digital pH-Meter, Metrohm AG, Herisau, Switzerland). Subsequently, the NaCl addition to all buffer solutions is adjusted with respect to the chloride already present to yield a total concentration of 0.1 M. All electrochemical experiments were performed with a microelectrochemical flow cell. This setup uses a 200- or 400- μm O-ring to confine the surface under investigation by pressing a capillary cell on the substrate with a well-defined force of 50 mN as monitored by a force sensor. The capillary itself is divided by a separating wall where one compartment holds the electrolyte supply channel and a $\mu\text{-Ag/AgCl}$ reference electrode [31], whereas the other holds the electrolyte drain and the Pt counter electrode. The cylindrical space created by the O-ring above the substrate provides the pathway for the electrolyte to flow from one compartment to the other at 0.26 $\mu\text{l s}^{-1}$. Precise determination of the size of the wetted area was performed in a separate experiment by optical recognition of color changes on tantalum thin films due to anodization to 10 V_{SHE} [32]. A detailed description of the scanning flow cell setup can be found in a former article [29]. Each experiment was carried out on an individual location on the substrate to ensure that the initial surface properties were identical for all measurements. The positioning and data acquisition process is fully automated using an in-house developed LabView program and did not require user interaction.

Online visible light spectroscopy (UV–VIS) The electrolyte from the exit side of the scanning flow cell was mixed with a complexing agent (0.2 mM ZINCON solution in 0.2 M borate buffer pH 9.25) and injected into a micro-transmission cell in Z-geometry. A tungsten halogen lamp and the detector (EPP 2000, StellarNet, USA) were connected using 300 μm optical fibers. The absorption at 580 nm was measured once every 1.2 s and transformed into a concentration using the proportionality factor as

determined by a calibration procedure with stock solutions. The delay time between tip of the capillary and detector was found to be 157 s at the applied solution flow rate. Further details about the setup and calibration procedure can be found in a former publication [29].

Scanning electron microscopy Scanning electron microscopy (SEM) was performed with an acceleration voltage of 12.0 kV using a Zeiss LEO 1550 VP scanning electron microscope. The magnification of all images shown in this study was chosen as 30k. All samples were thoroughly rinsed with ultrapure water prior to the imaging process to remove residual precipitates from the electrochemical experiments.

Results and discussion

Chemical etching of ZnO:Al thin films A series of measurement locations were chemically etched with 0.1 M acetate buffer possessing a chloride content of 0.1 M without applying any current. Four different etching solutions were prepared with pH values of 6.00, 6.50, 6.75, and 7.00. The zinc dissolution profiles during continuous solution flow are shown in Fig. 2. Each sample surface location was contacted by the microflow capillary for 1,000 s, followed by a purging step with the capillary off the surface for approximately 600–1,000 s.

All measurements were performed twice; both the shape and the integrals of the profiles obtained with identical parameters are highly reproducible. It is obvious that zinc exhibits a dissolution plateau with at least 85% of its final value reached within the first 200 s. The slight inclination

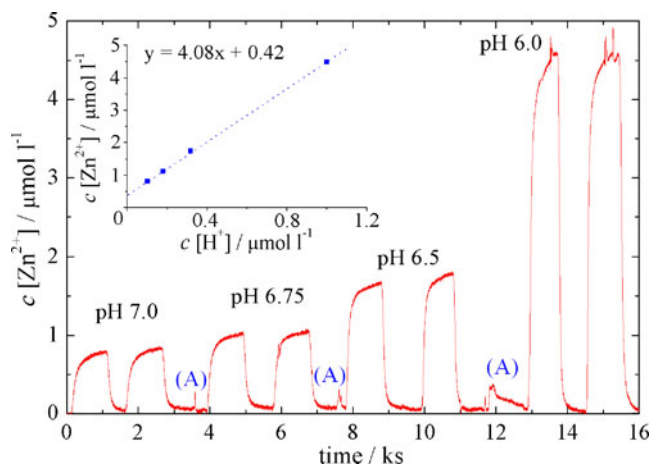
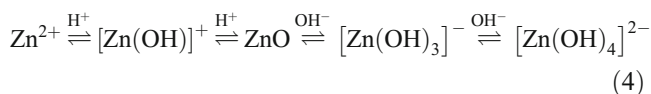


Fig. 2 Zinc dissolution profile during chemical etching in acetate buffers of different pH as measured by online UV–VIS spectrometry. The inset shows the zinc plateau concentrations versus the relative proton concentration; error bars are estimated from the deviation in the plateau region. The spikes in between measurements (A) originate from changing the solution

of the plateaus can be attributed to the non-quantitative transportation of zinc in the flow system, which slowly and linearly broadens the signal due to precipitation–dissolution reactions at the tube walls in addition to typical hydrodynamic peak broadening. The peaks during the non-contact time (A) are due to the exchange of the electrolyte during continuous flow. The decreasing pH causes a step-like increase in the solubility of zinc [33], so that residual zinc trapped in the flow system is immediately purged. Since the amount of Zn detected upon changing the electrolyte is minor, it has been neglected in the further discussion.

The height and the integrated area of the plateau of the characteristic concentration profiles of each location increase steadily with a decrease of the pH of the etching solution. Plotting the mean of the linear plateau regions versus the corresponding proton concentration yields a linear relationship in the inset of Fig. 2. This linearity at low dissolution rates appears reasonable considering the pH-dependent series of aqueous Zn species according to Ref. [19].



In near neutral or slightly acidic pH, the dissolution of ZnO to the mono-hydroxy complex is the dominant reaction and its formation kinetics is first order with respect to the proton concentration [15, 29]. The local depletion of protons at the electrode surface, which is of major importance for the chemical dissolution in near neutral pH, is reduced by the buffer system. This fact accounts for the steep slope in the inset of Fig. 2, where the dissolved zinc concentration exceeds the proton concentration by approximately a factor of 4. In order to investigate whether the reaction is under diffusion control despite the buffer effect, the acetate buffer concentration was varied in a further set of experiments (see Fig. 3).

The Zn concentration in the product stream dissolved from the surface increases with an increase in the buffer concentration. A linear relationship can be observed, which undoubtedly proves that the process is under transport control even at buffer concentrations up to 0.2 M. The wide region of transport control found by Guspil and Riesenkampf [34] up to 0.5 mM H₂SO₄ therefore applies for the present buffer systems as well. This further implies that chemical dissolution in the respective pH values between 6.0 and 7.0 is typically transport controlled also in the absence of a buffer system. In the latter case, however, the pH at the surface would immediately shift to alkaline due to the excessive proton consumption, leading to a drastic reduction in dissolution of Zn.

Besides the concept of proton transporting ions, also the chemical nature of the buffer itself affects the dissolution

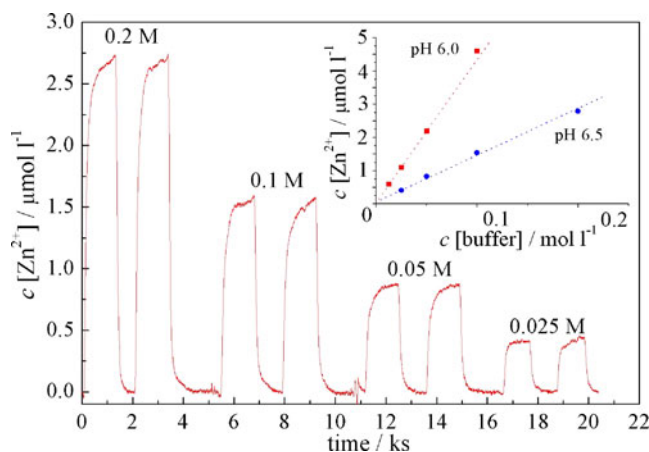


Fig. 3 Zinc dissolution profile during chemical etching in pH 6.5 acetate buffers of different concentrations. Inset Plot of the zinc plateau concentrations versus buffer concentration for pH 6.0 and 6.5

process and thus its rate. Acetate, which acts as a complexing agent for Zn ions, promotes the dissolution reaction [15] and therefore causes the linear fit in the inset of Fig. 2 not to cross the origin. The parallel background etching process can be estimated to about 0.4 μmol l⁻¹ in the experiment presented. The absence of this effect in Fig. 3 is caused by the fact that a lower buffer concentration both scales the proton and acetate induced dissolution, thus giving a linear fit crossing the origin.

The surface structure of the sample locations as determined by SEM after the chemical etching process for 1,000s at various pH values is shown in Fig. 4. A significant surface roughening occurred with structural features in the 100 nm range remaining. It appears that the surface topography is influenced by the grain boundaries initially present on the substrate, even though the etching process negatively influences the fineness of the structures displayed. Furthermore, for all etching parameters a mainly grooved surface develops with the original surface level still intact, only the sample treated with pH 6.0 displays harsh roughening also in depth (see Fig. 8). This can be considered as an intermediate situation compared to the topographies obtained by both HCl and KOH etching [16], as the high concentrations used in these processes merely form crater-like structures that exceed the grain size significantly. The surface topographies do not indicate a selective etching of particular grains, but rather a uniform etching starting from the grain boundaries. A preferential impact of the crystallographic orientation combined with the structural sensitivity of the reaction is not observed, due to the polycrystalline nature of the sample.

Electrochemical etching of ZnO:Al thin films The electrochemical etching process was performed by means of galvanostatic anodization at various current densities in 0.1 M NaCl. A matrix of locations on the substrate was

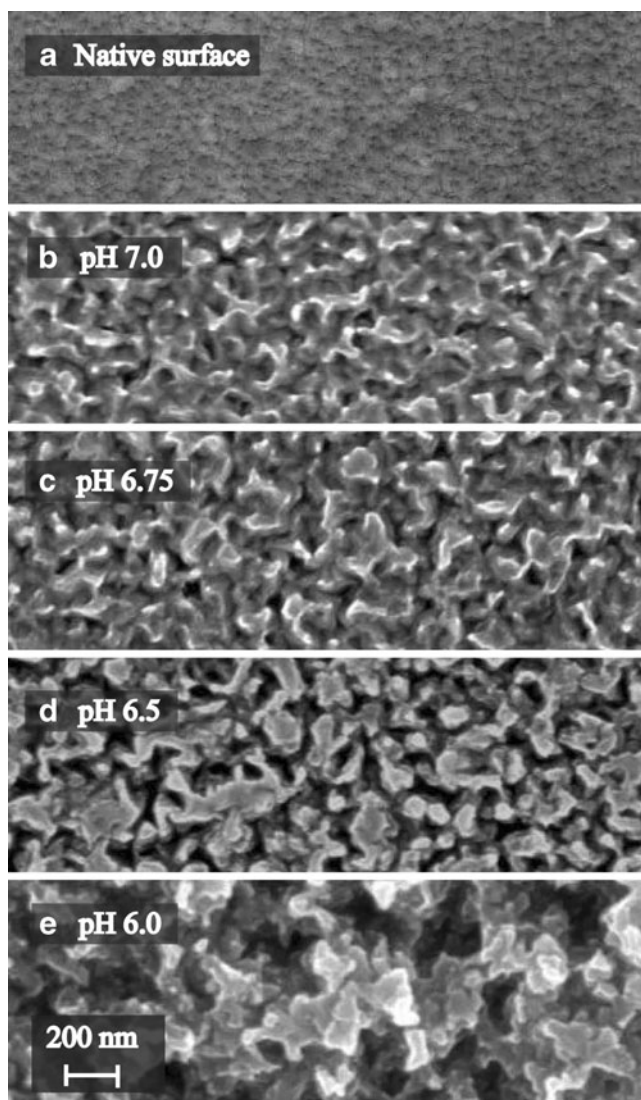


Fig. 4 SEM micrographs (mag. 30k) taken **a** before and **b–e** after 1,000 s of chemical etching in acetate buffers of various pH according to Fig. 1

programmed and automatically addressed with the scanning flow cell for 300 s each. Figure 5 shows two potential transients for each current density; the congruency of identical experiments again underlines the reproducibility of the method.

Initially, the potential transients for higher current densities rise sharply to certain peak potentials, which appear as plateaus at lower current densities, and then slightly drop again. After approximately 200 s, all potential transients reach quite stable values with increasing magnitude according to the applied current densities. These final potentials rest between 2.0 and 2.3 V_{SHE} , an indication for an early onset for film breakdown due to the high donor concentration in the thin ZnO layer [23]. Moreover, the narrow blocking region can also be attributed to the high impact of the grain boundary density on the anodization

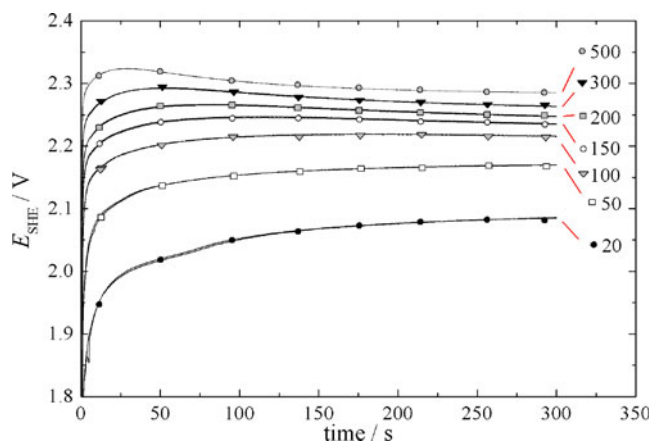


Fig. 5 Potential transients recorded during 300 s polarization of ZnO:Al in 0.1 M NaCl solution at different applied current densities ($\mu A\ cm^{-2}$; see inset)

behavior. To quantify the magnitude of film decomposition, zinc dissolution profiles were recorded in parallel and are shown in Fig. 6. The similarity between the electrochemical profile and the chemical dissolution shown in Fig. 2 is strong; the absence of an induction period for etching and the slight inclination of the plateau prove to be characteristic of the flow system. Both the chemical and electrochemical etching processes are therefore steady-state reactions given the electrolyte flow present in all experiments.

In the galvanostatic experiments, the consumed charge can be directly compared to the respective amount of Zn detected at the UV–VIS, evaluated by a numerical integration of the peak area. The linear relationship in Fig. 6b implies that the current efficiency for the anodic dissolution reaction is independent of the applied current density within the range of experimental parameters. In the case of 0.1 M NaCl solution, a slope of 0.88 corresponds to a current efficiency of 88%, whereas for the buffered solutions the current efficiency decreases to 62%. Note that the addition of a buffer reduces the current efficiency in the electrochemical experiment due to the scavenging of produced H^+ ions, in contrast to the chemical experiments where it provides a constant source of ions for the lattice attack. The shift in the axis intercept apparent in the latter systems originates from the chemical dissolution reaction that takes place in parallel to the electrochemical reactions during the experiment. The offset is proportional to the rate of chemical dissolution and corresponds well to the results presented in the former section.

Independent of a parallel chemical dissolution, electrochemically induced lattice decomposition (Eq. 2) and water oxidation (Eq. 3), with subsequent chemical etching due to a shift in the surface pH (Eq. 1), can be responsible for the dissolution of the ZnO thin film. These two reactions are in direct competition and most likely take place at the same

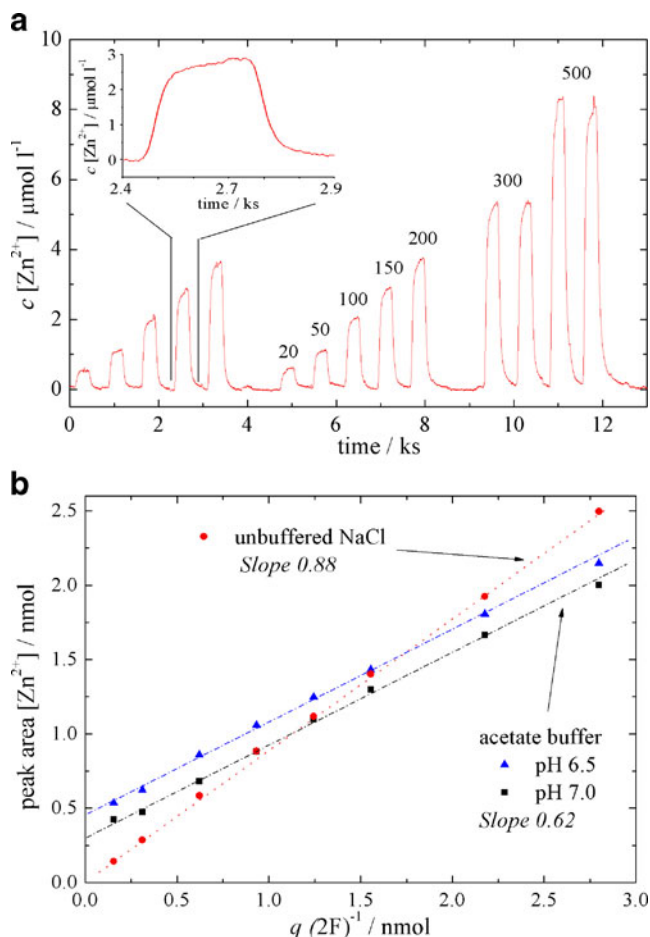


Fig. 6 **a** Zinc dissolution profiles recorded during galvanostatic anodization of ZnO:Al at different current densities (given in $\mu\text{A cm}^{-2}$) in unbuffered 0.1 M NaCl. **b** Plot of the peak integrals vs. applied charge divided by the Faraday constant and assuming a two-electron process for different electrolyte systems

active sites (e.g., points with the highest donor or defect density), the presented results suggest a coexistence of both processes. On the one hand, exclusive lattice decomposition can be excluded since the current efficiency for dissolution significantly deviates from 100%. Additionally, a buffer effect would not be expected in this case; however, it is clearly obvious from the decreasing slope in Fig. 6b. On the other hand, the water decomposition reaction itself strongly depends on the electrolyte system, especially the buffer capacity of the surrounding medium. If present exclusively, a largely suppressed Zn signal would be expected in the used buffer systems, since the buffer capacity exceeds the measured zinc concentrations (Fig. 6a) by approximately five orders of magnitude. More work, however, will be necessary to identify the exact mechanism or the individual contribution of these two possible pathways for the electrochemical ZnO dissolution.

Nevertheless, an immediate consequence of both reactions is a very high localization of the etching process to

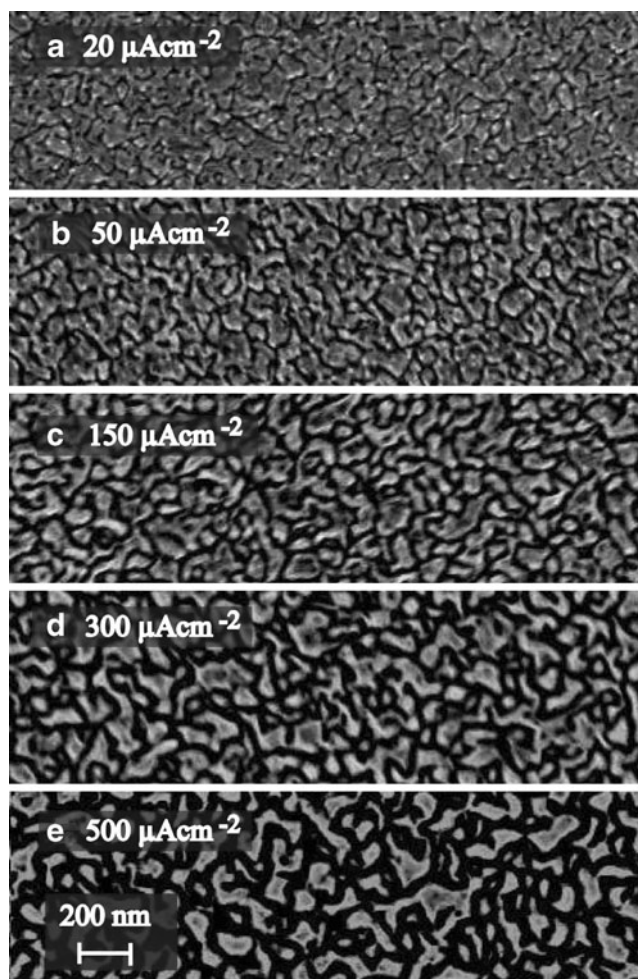


Fig. 7 SEM images of ZnO:Al thin film locations subject to 300 s of galvanostatic polarization in unbuffered 0.1 M NaCl solution after experiments with different current densities

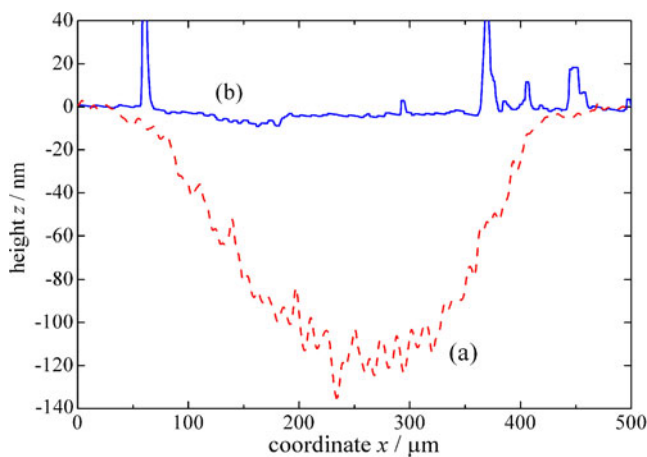


Fig. 8 Surface profile of a ZnO:Al surface chemically etched in 0.1 M NaCl solution with 0.1 M acetate buffer at pH 6.0 for 1,000 s (red dashed line) and electrochemically etched in an unbuffered 0.1 M NaCl solution at $500 \mu\text{A cm}^{-2}$ for 300 s (blue solid line) utilizing a 400- μm O-ring cell

areas of superior electrochemical activity. Certainly, this effect is evident for direct lattice decomposition, but must not be neglected also for surface pH changes even in buffered solutions. As a consequence, the selective removal of ZnO initiates and proceeds from the grain boundary sections [35], which becomes obvious from the images taken after experiments with different current densities in unbuffered NaCl solution in Fig. 7.

The electrochemical etching procedure is highly selective towards the grain boundaries, while in contrast to chemical etching the surface level seems to remain intact independent of the current density used. This predominant activity of the boundary sections together with their high density is also consistent with the early film breakdown behavior in the electrochemical experiments. Moreover, the electrochemically induced pH shift by water oxidation does not cause an integral change in the film thickness, the proton attack rather remains localized to the grain boundary regions. This close-range effect of the protons generated as well as the lattice decomposition was verified by profilometric measurements after electrochemical etching and compared to the chemical etching in Fig. 8.

The profilometric investigation with a needle of 25 μm in diameter is unable to resolve the local etching features at the grain boundaries in the nanometer range and therefore only displays the integral surface level. The original surface level appears nearly unchanged in the case of electrochemical etching despite the massive ZnO dissolution, which exceeds the chemical etch by approximately a factor of 2 in these particular experiments with the 400 μm O-ring cell (1.04 nM during chemical, 1.85 nM during electrochemical etching). This implies that the grooves in electrochemical etching must exhibit a very high aspect ratio reaching deep into the substrate. In contrast, the chemical etching in 0.1 M acetate buffer of pH 6.0 generates a pit due to a homogeneous removal of material, which qualitatively reflects the assumed flow velocity profile of the electrolyte in the capillary [36]. The observed spikes that are present in the region of the O-ring/surface contact result from disturbances of the probing needle by residual surface impurities most probably caused by precipitation reactions during the measurement and are not necessarily real topographical features of the ZnO:Al film. Very low scan speeds did lower, but not eliminate these signals.

In summary, galvanostatic etching of ZnO is a well-controllable and reproducible action that proceeds with high selectivity at grain boundaries. Since this technique can be easily combined with a conventional chemical etch, typical microscopic surface structures can thus be systematically refined on the nanoscale. The impact of these findings on the haze and light scattering capabilities of ZnO:Al thin

films and their relevance for solar cell applications will be investigated in a further study.

Conclusions

The chemical etching of RF-sputtered ZnO:Al at near neutral pH values was found to be diffusion-controlled even at high concentrations of acetate buffer (0.2 M), since the Zn dissolution rate increases linearly with the concentration of H^+ ions as well as of the buffer. The selectivity of the chemical etching towards the grain boundaries quickly vanishes as the rate increases, so that the dissolution becomes uniform over the whole surface.

The electrochemical etching procedure on the other hand dissolves ZnO with very high selectivity directly at the grain boundaries, which results from a direct lattice decomposition reaction and from local pH shifts due to water oxidation at these highly active sites. As a consequence, the electrochemically formed grooves demonstrate a very high aspect ratio depending on the applied current density and etching time.

The improved understanding of the different dimension of chemically etched pits and electrochemically corroded grain boundaries allows now for a combined, systematic approach to texture ZnO:Al thin films that will significantly contribute to the optimization of its optical properties for photovoltaic applications.

Acknowledgment The authors thank Janine Worbs (Forschungszentrum Jülich GmbH) for deposition of ZnO:Al thin films. Furthermore, the financial support by Dortmunder Oberflächencentrum GmbH, Dortmund, Germany and by the Deutsche Forschungsgemeinschaft (DFG, grant PU 447/1-1) is gratefully acknowledged.

References

- Lewis NS (2007) Toward cost-effective solar energy use. *Science* 315(5813):798–801
- Green MA (2006) Consolidation of thin-film photovoltaic technology: The coming decade of opportunity. *Prog Photovolt* 14(5):383–392
- Maycock PD (2005) PV review: World Solar PV market continues explosive growth. *Refocus* 6(5):18–22
- Kubon M, Boehmer E, Siebke F, Rech B, Beneking C, Wagner H (1996) Solution of the ZnO/p contact problem in a-Si:H solar cells. *Sol Energy Mater Sol Cells* 41–42:485–492
- Morris J, Arya RR, Odowd JG, Wiedeman S (1990) Absorption enhancement in hydrogenated amorphous silicon-based solar cells. *J Appl Phys* 67(2):1079–1087
- Müller J, Rech B, Springer J, Vanecek M (2004) TCO and light trapping in silicon thin film solar cells. *Sol Energy* 77(6):917–930
- Hüpkes J, Müller J, Rech B, Klein A, Rech B (2008) Texture etched ZnO:Al for silicon thin film solar cells. In: Ellmer K (ed) *Transparent conductive zinc oxide: basics and applications in thin film solar cells*. Springer, Berlin

8. Kluth O, Schöpe G, Hüpkes J, Agashe C, Müller J, Rech B (2003) Modified Thornton model for magnetron sputtered zinc oxide: film structure and etching behaviour. *Thin Solid Films* 442(1–2):80–85
9. Berginski M, Rech B, Hüpkes J, Stiebig H, Wuttig M (2006) Design of ZnO:Al films with optimized surface texture for silicon thin-film solar cells—art. no. 61970Y. In: Gombert A (ed) *Photonics for Solar Energy Systems*, vol 6197. Proceedings of the Society of Photo-Optical Instrumentation Engineers (Spie). Spie-Int Soc Optical Engineering, Bellingham, pp Y1970–Y1970
10. Owen JI, Hüpkes J, Zhu H, Bunte E, Pust SE (2011) Novel etch process to tune crater size on magnetron sputtered ZnO:Al. *Phys Status Solidi A* 208(1):109–113
11. Mariano AN, Hanneman RE (1963) Crystallographic polarity of ZnO crystals. *J Appl Phys* 34(2):384–388
12. Jo W, Kim S-J, Kim D-Y (2005) Analysis of the etching behavior of ZnO ceramics. *Acta Mater* 53(15):4185–4188
13. Gatos HC (1961) Dangling bonds in III–V compounds. *J Appl Phys* 32(7):1232–1234
14. Fruhwirth O, Herzog GW, Poulous J (1985) Dark dissolution and photodissolution of ZnO. *Surf Technol* 24(3):293–300
15. Gerischer H, Sorg N (1991) Chemical dissolution of oxides—experiments with sintered ZnO pellets and ZnO single crystals. *Werkst Korros Mater Corros* 42(4):149–157
16. Hüpkes J, Rech B, Calnan S, Kluth O, Zastrow U, Siekmann H, Wuttig M (2006) Material study on reactively sputtered zinc oxide for thin film silicon solar cells. *Thin Solid Films* 502(1–2):286–291
17. Lin YC, Jian YC, Jiang JH (2008) A study on the wet etching behavior of AZO (ZnO:Al) transparent conducting film. *Appl Surf Sci* 254(9):2671–2677. doi:10.1016/j.apsusc.2007.10.012
18. Valtiner M, Borodin S, Grundmeier G (2008) Stabilization and acidic dissolution mechanism of single-crystalline ZnO(0001) surfaces in electrolytes studied by in-situ AFM imaging and ex-situ LEED. *Langmuir* 24(10):5350–5358
19. Pourbaix M (1966) *Atlas of electrochemical equilibria in aqueous solutions*. Pergamon, New York
20. Gerischer H, Sorg N (1992) Chemical dissolution of zinc-oxide crystals in aqueous-electrolytes—an analysis of the kinetics. *Electrochim Acta* 37(5):827–835
21. Zembura Z, Burzynska L (1977) Corrosion of zinc in deaerated 0.1 M NaCl in pH range from 1.6 to 13.3. *Corros Sci* 17(11):871–878
22. Pettinger B, Schöppel HR, Gerischer H (1974) Tunnelling processes at highly doped ZnO electrodes in contact with aqueous electrolytes.1. Electron exchange with conduction band. *Ber Bunsen Ges Phys Chem Chem Phys* 78(5):450–455
23. Pettinger B, Schöppel HR, Yokoyama T, Gerischer H (1974) Tunnelling processes at highly doped ZnO-Electrodes in aqueous electrolytes. 2. Electron exchange with valence band. *Ber Bunsen Ges Phys Chem Chem Phys* 78(10):1024–1030
24. Wellings JS, Samantilleke AP, Warren P, Heavens SN, Dharmadasa IM (2008) Comparison of electrodeposited and sputtered intrinsic and aluminium-doped zinc oxide thin films. *Semicond Sci Technol* 23(12):7
25. Palacios-Lidon E, Perez-Garcia B, Vennegues P, Colchero J, Munoz-Sanjose V, Zuniga-Perez J (2009) Anisotropic chemical etching of semipolar 1011/ $\sqrt{101+1}$ ZnO crystallographic planes: polarity versus dangling bonds. *Nanotechnology* 20(6):6
26. Elias J, Tena-Zaera R, Wang GY, Levy-Clement C (2008) Conversion of ZnO nanowires into nanotubes with tailored dimensions. *Chem Mater* 20(21):6633–6637
27. Han J, Qiu W, Gao W (2010) Potential dissolution and photo-dissolution of ZnO thin films. *J Hazard Mater* 178(1–3):115–122
28. Yoo DG, Nam SH, Kim MH, Jeong SH, Jee HG, Lee HJ, Lee NE, Hong BY, Kim YJ, Jung D, Boo JH (2008) Fabrication of the ZnO thin films using wet-chemical etching processes on application for organic light emitting diode (OLED) devices. *Surf Coat Technol* 202(22–23):5476–5479
29. Klemm SO, Schauer J-C, Schuhmacher B, Hassel AW (2011) A Microelectrochemical Scanning Flow Cell with Downstream Analytics. *Electrochim Acta*, doi:10.1016/j.electacta.2011.01.052
30. Berginski M, Hüpkes J, Schulte M, Schöpe G, Stiebig H, Rech B, Wuttig M (2007) The effect of front ZnO:Al surface texture and optical transparency on efficient light trapping in silicon thin-film solar cells. *J Appl Phys* 101(7):074903–074911
31. Hassel AW, Fushimi K, Seo M (1999) An agar-based silver | silver chloride reference electrode for use in micro-electrochemistry. *Electrochem Commun* 1(5):180–183
32. Mardare AI, Hassel AW (2009) Quantitative optical recognition of highly reproducible ultrathin oxide films in microelectrochemical anodization. *Rev Sci Instrum* 80(4):046106. doi:04610610.1063/1.3117210
33. Reichle RA, McCurdy KG, Hepler LG (1975) Zinc hydroxide—solubility product and hydroxy-complex stability-constants from 12.5–75°C. *Can J Chem Rev Can Chim* 53(24):3841–3845
34. Guśpiel J, Riesenkampf W (1993) Kinetics of dissolution of ZnO, MgO and their solid-solutions in aqueous sulfuric-acid-solutions. *Hydrometallurgy* 34(2):203–220
35. Tuller HL (1999) ZnO grain boundaries: electrical activity and diffusion. *J Electroceram* 4:33–40
36. Lohrengel MM, Rosenkranz C, Klüppel I, Moehring A, Bettermann H, Van den Bossche B, Deconinck J (2004) A new microcell or microreactor for material surface investigations at large current densities. *Electrochim Acta* 49(17–18):2863–2870